


Nanobridge SQUIDs as Multilevel Memory Elements

Davi A.D. Chaves^{1,2,*}, Lukas Nulens², Heleen Dausy², Bart Raes², Donghua Yue²,
Wilson A. Ortiz¹, Maycon Motta¹, Margriet J. Van Bael² and Joris Van de Vondel^{2,†}

¹*Departamento de Física, Universidade Federal de São Carlos, São Carlos SP 13565-905, Brazil*

²*Quantum Solid-State Physics, Department of Physics and Astronomy, KU Leuven, Celestijnenlaan 200D, Leuven B-3001, Belgium*

 (Received 15 November 2022; revised 1 February 2023; accepted 3 February 2023; published 28 March 2023)

With the development of alternative computing schemes working at cryogenic temperatures, superconducting memory elements have gained interest. In this context, superconducting quantum interference devices (SQUIDs) are promising candidates, as they may trap different discrete amounts of magnetic flux. We demonstrate that a field-assisted writing scheme allows such a device to operate as a multilevel memory by the readout of eight distinct vorticity states at zero magnetic field. We present an alternative mechanism based on single phase slips, which allows the vorticity state to be switched while preserving superconductivity. This mechanism provides a possibly deterministic channel for flux control in SQUID-based memories, under the condition that the field-dependent energy of different vorticity states are nearby.

DOI: [10.1103/PhysRevApplied.19.034091](https://doi.org/10.1103/PhysRevApplied.19.034091)

I. INTRODUCTION

Multilevel memory systems are technologically appealing, for instance, due to an increase in storage density [1–3]. In recent years, alternative nonsemiconducting materials were proposed as nonvolatile multilevel memories in photonic [4] and antiferromagnetic [5] systems. In superconductors, a yTron current combiner can be used for nondestructive current readout and is capable of differentiating between discrete magnetic flux values trapped in superconducting loops [6], finding applications in proposed binary [7,8] and multilevel [9] memory elements.

Superconducting quantum interference devices (SQUIDs) are widely used as powerful magnetometers and are a driving force in the development of quantum technology [10–14]. In a conventional SQUID, superconductor-insulator-superconductor junctions present a sinusoidal current-phase relationship ($C\Phi R$) leading to a periodic single-valued dependence between the device critical current I_c and the applied magnetic field B . However, if at least one of the junctions is an elongated constriction, such as a nanobridge or a nanowire, the $C\Phi R$ of the junction becomes linear [15,16]. As a result, the $I_c(B)$ oscillations become linear as well and the four line segments of $I_c(B)$, two in the positive and two in the negative current side, define a so-called vorticity diamond [17,18].

Additionally, the superconducting phase across such elongated constrictions can exceed 2π [18]. As such, different solutions exist at one magnetic field value (overlap of the vorticity diamonds), each corresponding with a different winding number, n_v , of the superconducting phase across the SQUID. Moreover, each vorticity state is characterized by a particular energy and critical-current value. Therefore, a critical-current measurement is a reliable tool to distinguish between different vorticity states. Finally, a single or series of topological fluctuations will trigger a transition to a different vorticity state or to the normal state by locally suppressing the order parameter, causing the phase across that given region to change by an integer multiple of 2π [19–23]. These events are known as phase slips.

The SQUID vorticity may be set to a predetermined value by the establishment of proper writing protocols [24–26]. This implies that information can be stored in the SQUID's different vorticity states. Indeed, flux-based qubits and memory elements relying on phase-slip physics have already been proposed [20,26–30]. In this context, an applied magnetic field affects the SQUID energy and is a natural choice of control parameter in a flux-based memory. By providing a straightforward manner of changing the trapped flux inside a superconducting ring, it allows changing vorticities via phase slips. Recently, the role played by the field-dependent SQUID energy in the phase-slip phenomena has gained attention. It was demonstrated that applied transport currents flowing in SQUIDs subjected to constant magnetic fields can also induce a transition between different vorticity states [31]. This fact

*davi@df.ufscar.br

†joris.vandevondel@kuleuven.be

has been explored in proposed zero-field memory elements [26,29], in which the key ingredient is the creation of an asymmetry in the superconducting properties of the SQUID junctions. For a fully superconducting device, we previously demonstrated that the kinetic induction of the junctions may be tuned via nanofabrication, allowing control over the $I_c(B)$ characteristics of the device [18].

In this paper, we report on the feasibility of SQUIDs containing nanobridges as multilevel memory elements. We demonstrate that by defining a field-assisted writing protocol, a large number of vorticity states can be accessed and then read at zero applied field, effectively creating an eight-level memory system. However, writing to a specific state relies on a probabilistic process that requires the vorticity to be frozen in a determined state as the device transitions from the normal to the superconducting state. This process is heavily influenced by the total SQUID energy, an ingredient overlooked in previous studies. Using this information, we demonstrate that at applied fields for which adjacent vorticity states have equal energy, there is a very high probability of changing vorticity via single phase slips. By not triggering an unwanted transition out of the superconducting state, this mechanism constitutes an alternative and possibly deterministic channel for flux control.

II. EXPERIMENTAL DETAILS

The samples investigated in this work are asymmetric Au-capped $\text{Mo}_{78}\text{Ge}_{22}$ nanoSQUIDs comprised of one Dayem bridge (DB) and one 40-nm-wide nanobridge (NB) of lengths varying from 100 to 400 nm. Figure 1(a) shows the SEM image of a prototypical device. To illustrate our discussion, we report on three selected samples, labeled devices 250, 400a, and 400b according to the nominal length of the nanobridge. Devices 400a and 400b share the same geometry. By changing the NB length, we effectively control the superconducting properties of the junctions [18]. The devices are patterned using standard e-beam lithography. A 22-nm-thick $\text{Mo}_{78}\text{Ge}_{22}$ layer is deposited in a high-vacuum pulsed-laser deposition chamber and the resulting structures are capped with a 3-nm-thick gold layer to prevent oxidation. Critical-current values were extracted from standard VI measurements using the four-point probe method, as shown schematically in Fig. 1(a). During experiments, samples are kept in an Oxford Instruments Heliox ^3He cryostat at a base temperature of 300 mK. A room-temperature π filter with a cutoff frequency of 1 MHz and a Stanford Research Systems SR560 low-noise preamplifier are used in the measurements.

III. FIELD-ASSISTED WRITING: THE SQUID AS A MULTILEVEL MEMORY ELEMENT

Initial $I_c(B)$ characterizations for device 400a are performed as presented in Fig. 1(b). These measurements,

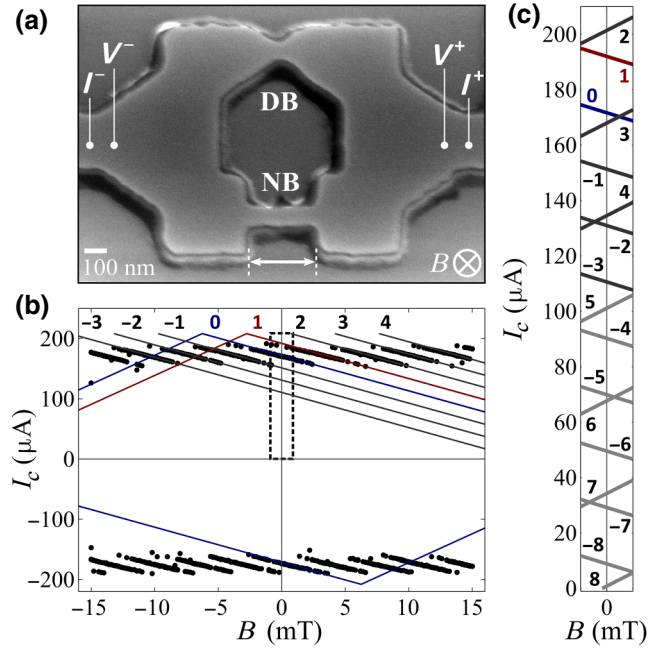


FIG. 1. (a) SEM image of a representative asymmetric $\text{Mo}_{78}\text{Ge}_{22}/\text{Au}$ SQUID with nominal nanobridge length of 300 nm and width of 80 nm. (b) Characteristic $I_c(B)$ distribution for device 400a at 300 mK. The points are gathered during three different sweeps for each magnetic field value and for each current direction. Numbered lines are fits of the vorticity diamond branches—the left-side branch is shown only for $n_v = 0$ and 1 for simplicity. (c) The vorticity diamonds for $-8 \leq n_v \leq 8$ in the region around 0 mT defined by the dashed rectangle in (b).

collected in three independent runs, allow the identification of different vorticity states based on their corresponding critical-current values. The fit of $I_c(B)$ is performed following Eq. (A1) and is represented by the numbered lines for different n_v states in Fig. 1(b) [32]. As defined in Appendix A, the results for device 400a reveal values of $\Delta B = 3.5 \pm 0.1$ mT, $I_c^{NB} = 101.5 \pm 0.3$ μA , $I_c^{DB} = 106.7 \pm 0.6$ μA , $\varphi_c^{NB} = 31.3 \pm 0.4$ rad, $\varphi_c^{DB} = 20.1 \pm 0.6$ rad, $L_k^{NB} = 102 \pm 1$ pH, and $L_k^{DB} = 62 \pm 2$ pH, indicating a significant difference in the properties of the junctions.

These parameters allow us to trace the complete vorticity diamonds for device 400a, extrapolating the regions in the $I_c(B)$ distribution where critical-current measurements of a specific state are favored. For simplicity, Fig. 1(b) shows only the four diamond branches for $n_v = 0$. The choice for a very long nanobridge is based on the knowledge that such a constriction would present a large critical phase and kinetic inductance [18]. As a consequence, a large number of states is expected to be found at a given applied field. Figure 1(c) highlights the region delimited by the dashed rectangle in (b) showing the vorticity diamonds for $-8 \leq n_v \leq 8$ around 0 mT. We observe that, although our initial experimental data reveals only two states at zero

field, 17 total vorticities are expected to exist on the positive current side of the $I_c(B)$ distribution, supporting our design choices. To explore this rich landscape two things are paramount: the ability to write, i.e., select, the device vorticity state n_v ; and the possibility to perform a readout of that state in a determined field value.

The acquired $I_c(B)$ information can be used to implement a writing (or preparation) protocol that allows one to actively choose the device vorticity state [17,31,33]. To illustrate this, consider Fig. 2(a). It shows the critical current obtained for device 400a after performing 1500 I_c measurements at zero magnetic field. Comparing the results with the $I_c(B)$ distribution of Fig. 1(b) we can identify only $I_c(0)$ values representing vorticity states $n_v = 1$ ($I_{c,1} \sim 192 \mu\text{A}$, with a probability of 11%) and $n_v = 0$ ($I_{c,0} \sim 172 \mu\text{A}$, 89%). These probabilities are dictated by the stochastic freeze-in process that determines the SQUID vorticity after entering the superconducting state at zero field. Notice that the highest I_c state, $n_v = 2$, is never observed. This is associated to the fact that, for sufficiently asymmetric SQUIDs [18,26], the highest I_c state is not energetically favored when entering the superconducting state at zero magnetic field, as it presents a higher total energy than $n_v = 0$ —see Appendix B. Figure 2(b) then shows the $I_c(B)$ distribution around the positive peaks of $n_v = 0$ and 1, highlighting their zero-field critical currents, $I_{c,0}$ and $I_{c,1}$. Figure 2(c) shows how a bias current I^* may be used to gauge the SQUID vorticity. If $I^* < I_{c,0}$, as represented by the blue region, it is not possible to distinguish between $n_v = 0$ and $n_v = 1$, as both are possible at such bias current and the device will remain in the superconducting state regardless. However, if $I_{c,0} < I^* < I_{c,1}$ the device will remain superconducting if it is found in $n_v = 1$, but will transition to the normal state if it was previously in $n_v = 0$. For the latter case, if the current is then reduced to zero, re-establishing superconductivity, the resulting vorticity state is dictated by the stochastic process with probabilities revealed by Fig. 2(a). Therefore, the protocol to write device 400a in $n_v = 1$ consists of looping the current between zero and $I_{c,0} < I^* < I_{c,1}$ until the voltage V_S across the device reads zero at I^* , i.e., it is in the superconducting state. The same principle is used in combination with a bias magnetic field, B^* , to successfully prepare the device in different states [31].

The use of our devices as memory elements requires the ability to reliably read different prepared states at the same applied magnetic field. To illustrate this, we prepare device 400a in different vorticity states using the coordinates presented in Table I. By first reducing the bias current and then the bias field to zero, thus never leaving the constraints of the vorticity diamond, we are able to preserve the prepared states at zero magnetic field. Figure 2(d) reveals that the readout is successful at 0 mT for $-3 \leq n_v \leq 4$. It shows eight different histograms, each containing 100 I_c measurements after preparing the device in the

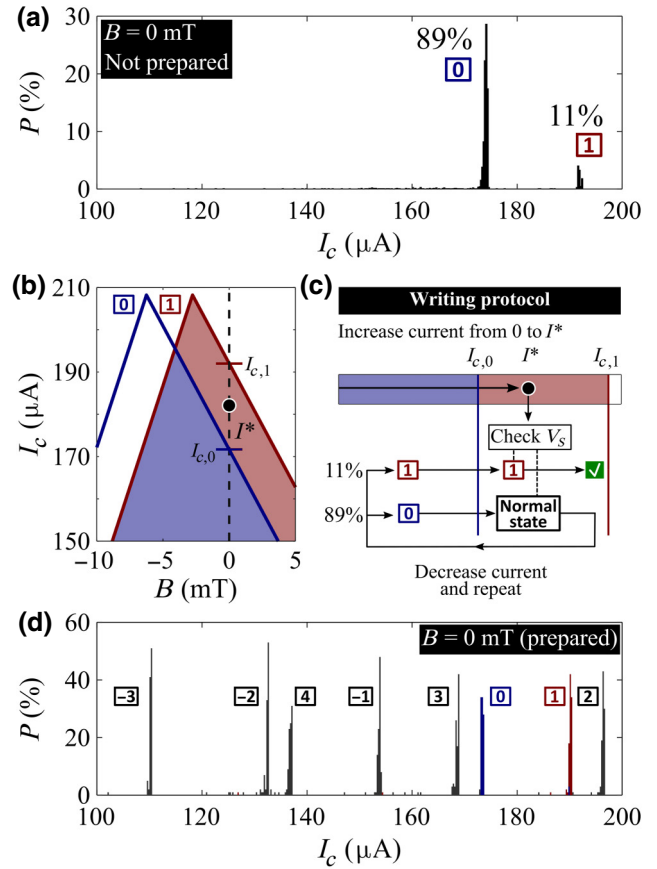


FIG. 2. (a) Critical-current distribution for device 400a after 1500 measurements at zero magnetic field when the vorticity state is frozen in during a cool down from $+220 \mu\text{A}$, i.e., without preparing the device in any specific state. (b) Detail of the $I_c(B)$ distribution showing the vorticity diamond fit for $n_v = 0$, blue solid line, and $n_v = 1$, red solid line. The value of I^* is chosen such that $I_{c,0} < I^* < I_{c,1}$. (c) Schematic representation of the writing protocol for vorticity state $n_v = 1$. Repeatedly applying a current between 0 and I^* will prepare the system in $n_v = 1$. To gauge if the preparation is successful, the voltage V_S across the device is checked with the current set at I^* . If V_S reveals the SQUID is in the normal state, current should be reduced to zero, restoring the superconducting state, and the procedure repeated. If $V_S = 0$, then the SQUID is in state $n_v = 1$ and the preparation is successful. (d) I_c distributions at zero magnetic field after preparing the device in different vorticity state. All measurements are performed at 300 mK.

corresponding state before each current sweep. The observed critical currents are as low as $I_{c,-3} \sim 112 \mu\text{A}$ and as high as $I_{c,2} \sim 198 \mu\text{A}$ —a variation of over 76% and an enhancement of approximately 14.8% for $I_{c,2}$ in comparison with $I_{c,0}$. The measurements in Fig. 2(d) show close agreement with fits of the vorticity diamonds at zero field presented in Fig. 1(c). State $n_v = 5$, on its turn, could not be read at zero field, as the same 100 measurements yielded I_c readings representing states $n_v = -3, -2$, and -1 . This fact is related to Joule heating. For the previous eight

TABLE I. Bias current (I^*) and magnetic field (B^*) used in the field-assisted preparation protocol for device 400a.

n_v	-3	-2	-1	0	1	2	3	4	5
B^* (mT)	-13	-10	-6.5	-3.7	0	3.7	6.5	10	13.5
I^* (μ A)	178	178	178	180	180	183	183	183	183

states, with higher I_c , as the current is swept across the diamond edge, the heat dissipated by phase slips is large enough so that the device could not re-establish the superconducting state. For $n_v = 5$, and all subsequent lower I_c states, this is not the case. As the current reaches the diamond edge, a phase slip will occur without causing a cascade transition to the dissipative state. In other words, during the readout the vorticity is altered by a nonobservable, or hidden phase slip. As such, no reliable reading is possible for these states at 0 mT. Figures 2(a)–2(d) also reveal around 5% of I_c readings that cannot be traced to any specific n_v . These are random errors related to voltage fluctuations in the measurement setup that can be reduced by better line filtration.

This analysis reveals the ability of our SQUID to behave as an eight-level memory, i.e., it presents eight different nonvolatile states that can be read at a fixed magnetic field. Differently from a recently proposed memory element that relies on the physics of a single elongated weak link [30], the writing between different states in Fig. 2(d) is not a direct process, i.e., it does not require one sole physical stimulus like one magnetic field pulse. On the other hand, it is only by embedding the nanobridge in a SQUID that the possibility of exploring the physics of the weak link to create a multilevel memory element arises. Moreover, the total number of available states depends decisively on three factors: (i) the slope of the vorticity diamond, tuned by the NB length; (ii) the device's critical current; and (iii) the maximum current for which the device can recover from a phase slip without triggering a transition to the normal state. Therefore, it is possible to develop memory elements suited for specific needs by appropriate material and design choices. These are remarkable features that can only be accessed by the use of magnetic fields in the writing protocol and may be explored for sensing applications and in the development of nonvolatile multilevel memory elements.

IV. TOWARDS NONPROBABILISTIC VORTICITY STATE SWITCHING

The fact that the writing process depicted in Fig. 2(c) is probabilistic is a major downside in comparison to alternative deterministic memory systems. Although a probabilistic writing scheme has been used previously in proposed memory elements [26], it is paramount to move towards a viable vorticity state switch protocol that does not rely on the process of leaving and returning to the superconducting

state. Moreover, simply reducing the width of applied current pulses to manipulate the state does not solve the issue. As we demonstrate in Sec. III, the frozen-in vorticity when the SQUID enters the superconducting state depends decisively on the device energy. In asymmetric SQUIDs [26], as our own, the lowest energy state may not present the highest I_c at a desired applied field, hampering the writing process.

Fortunately, it is possible to influence the probability of changing states without triggering irreversible heating to the dissipative state by exploring single phase slips—if an applied magnetic field is used to favorably bias the energy [31]. Figure 3(a) presents the energy versus magnetic field behavior at zero bias current obtained from the kinetic inductance values for device 400a for $n_v = 0$ and 1 according to Eq. (B1). The field-dependent absolute energy difference between the states, labeled as $|\Delta E_{0,1}|$, is highlighted in the panel. At zero field, the energy values $E_0^{n_v}$ increase parabolically with n_v . As such, $E_0^0 = 0$ represents the more energetically favorable configuration for the investigated SQUID, as shown in Appendix B, which helps to explain why the probability that device 400a freezes in $n_v = 0$ is the highest when entering the superconducting state at zero field. Accordingly, the only other observed state, $n_v = 1$, presents the second lowest energy at 0 mT and, therefore, the second highest probability. The possibility that a metastable energy state appears in the measurements is related to random fluctuations experienced while the device enters the superconducting state [31]. Figure 3(b) shows a schematic representation of the energy landscape around vorticity states $n_v = 0$ and 1 at selected magnetic fields. Finally, although $E_0^{+1} = E_0^{-1}$, $n_v = -1$ is not observed in Fig. 2(a). This happens because there is a dependence of the current polarity on the freeze-in probability, which is tied to the shape of the vorticity diamonds and can be attested in Fig. 1(b) by noting that, for the negative current measurements, it is $n_v = -1$ and not $n_v = 1$ that is observed at zero field.

Figure 3(c), meanwhile, reveals an intriguing feature. When the device is prepared in $n_v = 0$, there is a defined field region, highlighted by the gray shaded area, showing a predominant probability of observing a single phase slip changing the vorticity of the SQUID to $n_v = 1$. This is demonstrated in the main panel by one representative field-dependent I_c measurement in which device 400a is prepared in $n_v = 0$ prior to a current sweep at each field value—solid blue points [34]. The blue and red solid lines are fits of Eq. (A1) for the vorticity diamonds for states $n_v = 0$ and 1, respectively. Considering the blue points, for the left-most field values, the observed critical currents correspond to that of the prepared state, $n_v = 0$. As the field is increased towards and beyond the line at $B = 1.74$ mT, at which $E_B^{+1} = E_B^0$, a current sweep may induce a single phase slip and the observed I_c now corresponds to that of $n_v = 1$. For measurements at even higher fields, device

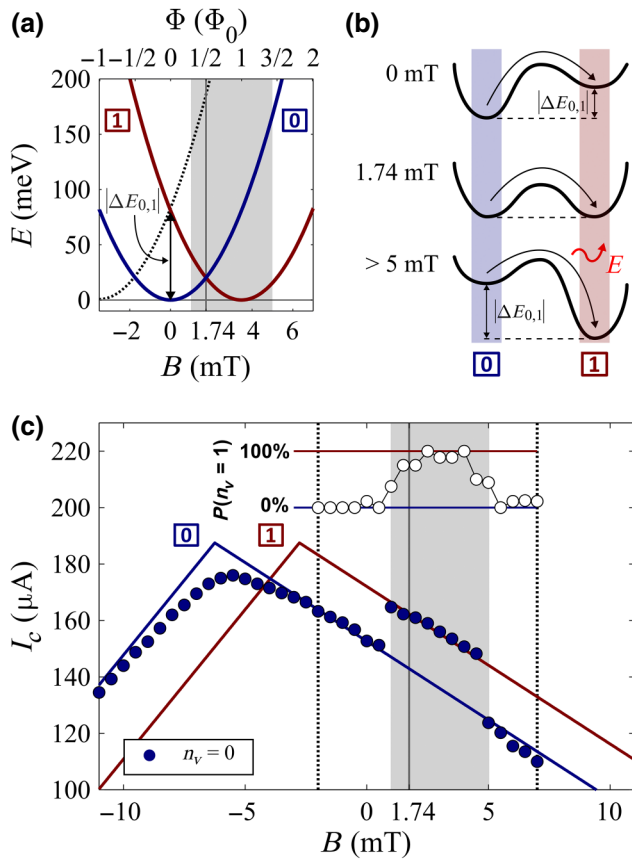


FIG. 3. (a) Energy versus magnetic field at zero current bias for $n_v = 0$ and 1 for device 400a obtained from the kinetic inductance. The dotted curve represents the energy for $n_v = -1$. (b) Schematic representation of the energy landscape around the minima at $n_v = 0$ and 1 at selected applied fields. The absolute energy difference $|\Delta E_{0,1}|$ is represented along a pictorial view of the energy barrier between the states. Curved dark arrows indicate the switch from state $n_v = 0$ to 1 and the red arrow highlights the energy dissipated by one such phase slip at high applied fields. (c) Main panel shows one representative $I_c(B)$ measurement after preparing device 400a in $n_v = 0$ at 300 mK. The respective vorticity diamonds for states $n_v = 0$ and 1 are shown as solid lines. The inset shows the probability of finding the device in $n_v = 1$ after a current sweep at particular field values as averaged for nine different measurements. In (a) and (c), a gray shaded area highlights the field values for which there is a high probability of observing single phase slips from $n_v = 0$ to $n_v = 1$.

400a no longer experiences single phase slips and again the readout corresponds to the state $n_v = 0$. This experiment is repeated nine times in the field region between the two dotted lines in Fig. 3(c). The averaged probability of finding device 400a in state $n_v = 1$ after the current sweep is plotted in the inset. It shows that, at particular field values, the device will mostly endure a single phase slip to $n_v = 1$ instead of transitioning to the normal state.

Such an observation may be better understood with the help of Fig. 3(b). At zero field, there is a nonzero energy difference between states $n_v = 0$ and $n_v = 1$ for device 400a. On top of that, switching from $n_v = 0$ to $n_v = 1$ requires the SQUID to surpass a characteristic energy barrier. Then, as the current is swept across the edges of the vorticity diamond of $n_v = 0$ at 0 mT, a phase slip to $n_v = 1$ will not occur, as it would strongly increase the energy of the system, and the normal state would be recovered. However, as the magnetic field is increased, $|\Delta E_{0,1}|$ decreases. At an applied field corresponding to $\Phi_0/2$, or 1.74 mT, $|\Delta E_{0,1}| = 0$. For $B > 1.74$ mT, $n_v = 1$ presents the lowest energy and is thus the favorable state, as seen in Fig. 3(a). Inspection of Fig. 3(c) reveals that around such an applied field, device 400a will mainly be found at $n_v = 1$ after the current sweep. This is now the case because the energy released by a phase slip is lower than that required to switch from $n_v = 0$ to $n_v = 1$ at 0 mT, and the SQUID may sustain it while remaining in the superconducting state. As $|\Delta E_{0,1}|$ becomes small, this reasoning explains why a number of energy-increasing phase slips are observed as B approaches 1.74 mT. An analogous behavior is reported by Ref. [31]. As the field is increased above 1.74 mT, $|\Delta E_{0,1}|$ increases, ultimately causing a phase slip from $n_v = 0$ to $n_v = 1$ to release enough energy to again drive the device out of the superconducting state. For that reason, the observed vorticity state switch from $n_v = 0$ to $n_v = 1$ is not present at fields higher than 5 mT in Fig. 3(c).

A second SQUID containing a 400-nm-long NB, labeled device 400b, is studied. Completely analogous results are found and are shown in Appendix C. Moreover, for device 400b, we observe that preparation in all states between $-2 \leq n_v \leq 2$ results in a similar behavior, i.e., there are contained field regions that favored phase slips increasing the vorticity of the SQUID by $+1$. This suggests an alternative, step-by-step, vorticity state switching mechanism with very high probabilities, possibly even deterministic. Based on single phase slips, such mechanism would also present the benefit of not requiring leaving the superconducting state, thus reducing dissipation during memory operation.

Of note, this mechanism appears to be unidirectional in n_v , as we are not able to observe the reverse process in phase slips that decrease the vorticity. We can understand this considering the $I_c(B)$ distribution in Fig. 1(b). If device 400a is initially prepared in $n_v = 0$, one could expect a high probability to observe phase slips to $n_v = -1$ at -1.74 mT, corresponding to $-\Phi_0/2$ —see the dotted curve in Fig. 3(a). However, around such an applied field, $n_v = -1$ has a lower I_c than $n_v = 0$. It is then impossible for the vorticity to change to $n_v = -1$ after the current is swept across the positive side of the vorticity diamond of $n_v = 0$ and the device will transition to the dissipative state. Moreover, at zero field, such phase slips may compromise the readout of the prepared state, therefore

an optimal device design is required. As such, the exploration of the presented effect as an alternative, possibly deterministic, and tunable flux control mechanism is an enticing possibility for the development of superconducting memory elements. In this effort, we find that a long NB is a necessity. While longer NBs consistently present particular regions with high single phase-slip probabilities, measurements conducted for devices containing 250-nm (see Appendix C) and 300-nm NBs did not show such regions. Inspection of the energy versus field behavior of these samples does not reveal a significant difference in comparison with what is shown in Fig. 3(a) for device 400a. Therefore, an approach capable of resolving the dynamics of the system and the role of the characteristic energy barrier between adjacent vorticity states is needed to explain our experimental observations for shorter NBs.

V. CONCLUSIONS

We fabricate different fully superconducting Mo₇₈Ge₂₂ SQUIDs comprised of one Dayem bridge and one nanobridge. Due to the tailored properties of the junctions, multiple vorticity diamonds intersect the zero-field line in the $I_c(B)$ distribution of our devices, which can be further influenced by the modification of the nanobridge length, an effective control parameter of the superconducting properties of the junctions. The implementation of a field-assisted writing protocol allows reliable access to eight different vorticity states with distinct macroscopic properties at zero applied magnetic field, revealing the potential of our device as a superconducting multilevel memory element. An alternative approach to effectively switch the SQUID vorticity state by one winding number is presented, as for long enough nanobridges we demonstrate the existence of particular field regions where a current sweep favorably induces a single phase slip to the next vorticity state. Our analysis points to the determinant role played by the SQUID energy in the mechanisms involved in the freeze-in and phase-slip probabilities, indicating applied magnetic fields as a vital ingredient in the effective manipulation of the vorticity states.

ACKNOWLEDGMENTS

This work is supported by Coordenação de Aperfeiçoamento de Pessoal de Nível Superior—Brasil (CAPES)—Finance Code 001, the São Paulo Research Foundation (FAPESP, Grant No. 2021/08781-8), the National Council for Scientific and Technological Development (CNPq, Grants No. 316602/2021-3, and No. 309 928/2018-4), the China Scholarship Council (No. 202004 890002), Research Foundation Flanders (FWO, Belgium, Grants G0A0619N, G0D5619N, and 11K6523N), and by COST action SUPERQUMAP (Grant No. CA21144). D.A.D.C. acknowledges Capes-PDSE Grant No. 88881.624531/2021-01.

APPENDIX A: VORTICITY DIAMONDS

To obtain reliable readings of the SQUID vorticity states, it is necessary to have prior knowledge of their respective critical currents for different applied fields. For the SQUIDs employed in this work, we may consider the junctions to present linear CΦRs of the form $I_c^{NB,DB} = I_c^{NB,DB} (\varphi_c^{NB,DB} / \varphi_c^{NB,DB})$, where $I_c^{NB,DB}$ is the supercurrent and $\varphi_c^{NB,DB}$ the critical phase difference across the nanobridge and the Dayem bridge, respectively [18]. The left- and right-side linear segments of the positive current side of $I_c(B)$ are then given by

$$\begin{aligned} I_c^{\text{left}}(B) &= I_c^{NB} \\ &+ \left(\frac{\Phi_0}{2\pi L_k^{DB}} \right) \left(\varphi_c^{NB} + 2\pi \frac{B}{\Delta B} \right), \\ I_c^{\text{right}}(B) &= I_c^{DB} \\ &+ \left(\frac{\Phi_0}{2\pi L_k^{NB}} \right) \left(\varphi_c^{DB} - 2\pi \frac{B}{\Delta B} \right), \end{aligned} \quad (\text{A1})$$

where Φ_0 is the magnetic flux quantum, $L_k^{NB,DB}$ the kinetic inductance of the junction, and ΔB is the Little-Parks oscillation period defined by the area of the SQUID loop as $\Delta B = \Phi_0 / A_{\text{loop}}$.

APPENDIX B: SQUID ENERGY

The ability to write the device to a specific state is a process related to the SQUID energy, as a freeze-in from the normal to the superconducting state will favor stable (less energetic) states over metastable ones [31]. Then, by neglecting the self-inductance contribution estimated to be around 30 to 50 times smaller for a loop with the dimensions of our devices [18], the total energy stored in the SQUID depends on the the bias current I_{bias} and the magnetic field as [31]

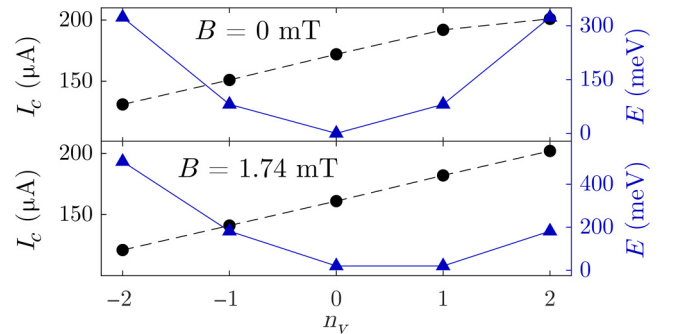


FIG. 4. Evolution of the critical current (dark circles) and total SQUID energy (blue triangles) as a function of n_v for different applied magnetic fields at 300 mK.

$$E_B^{n_v} = \frac{1}{2} \left(\frac{L_k^{NB} L_k^{DB}}{L_k^{NB} + L_k^{DB}} \right) I_{\text{bias}}^2 + \frac{1}{2} \frac{1}{L_k^{NB} + L_k^{DB}} \left(\frac{B}{\Delta B} \Phi_0 - \Phi_0 n_v \right)^2, \quad (\text{B1})$$

where n_v is the vorticity state given by the relationship $\varphi^{NB} - \varphi^{DB} + 2\pi B/\Delta B = 2\pi n_v$, which represents the single valuedness of the superconducting order parameter [18].

For a given applied magnetic field, the lowest energy state may not be the one presenting the highest critical current. To illustrate such a situation for device 400a, Fig. 4 shows I_c and E at $B = 0$ mT and $B = 1.74$ mT as a function of n_v . The values represented are obtained from the fit of the vorticity diamonds and from Eq. (B1). In both cases, $n_v = 2$ presents the highest I_c value, while $n_v = 0$

and $n_v = 1$ have a lower total energy and $n_v = -1$ also has a lower energy at 0 mT. This picture can be understood following Fig. 3(a) and knowing that $E(B)$ for $n_v = -1$ and 2 are symmetric around 1.74 mT.

APPENDIX C: DIFFERENT DEVICES

Figure 5 presents results obtained for devices different from the one discussed in the main text. Figure 5(a) demonstrates that, around $\Phi_0/2$, or 1.74 mT, device 400b shows an increased probability of experiencing single phase slips from $n_v = 0$ to $n_v = 1$. This confirms the findings described in Sec. IV for device 400a. Moreover, it also shows a completely analogous behavior at $3\Phi_0/2$, or 5.22 mT, at which field $|\Delta E_{1,2}| = 0$. If device 400b is prepared in $n_v = 1$, it presents a high probability of experiencing a single phase slip to $n_v = 2$. Figure 5(b) presents data for a device containing a shorter, 250-nm NB. No phase slips are observed as the current is swept across the vorticity diamond of the prepared state $n_v = 0$. Therefore, we demonstrate that a long nanobridge is needed to create single-phase-slip-favorable field regions, as discussed in Sec. IV.

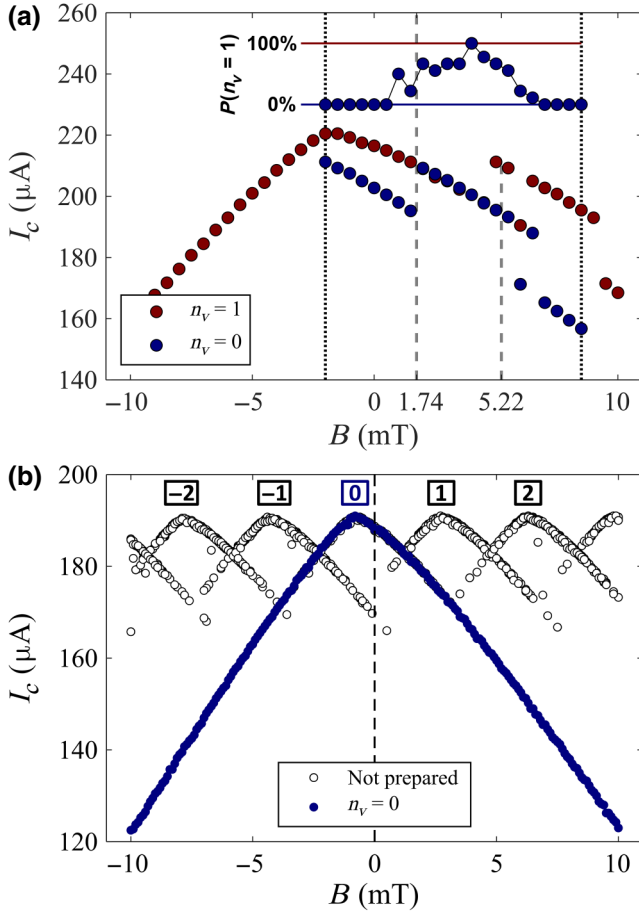


FIG. 5. (a) Main panel shows representative $I_c(B)$ measurements after preparing device 400b in $n_v = 0$ and $n_v = 1$. The inset shows the probability of finding device 400b in $n_v = 1$ after a current sweep at particular field values after it is initially prepared in $n_v = 0$. The presented values are averaged from nine different measurements. (b) $I_c(B)$ for device 250 when no preparation protocol is performed and after preparing in $n_v = 0$ before each measurement. All measurements are performed at 300 mK.

- [1] M. J. Rozenberg, I. H. Inoue, and M. J. Sanchez, Non-volatile Memory with Multilevel Switching: A Basic Model, *Phys. Rev. Lett.* **92**, 178302 (2004).
- [2] R. Waser, R. Dittmann, G. Staikov, and K. Szot, Redox-based resistive switching memories—nanoionic mechanisms, prospects, and challenges, *Adv. Mater.* **21**, 2632 (2009).
- [3] F. Zahoor, T. Z. Azni Zulkifli, and F. A. Khanday, Resistive random access memory (RRAM): An overview of materials, switching mechanism, performance, multilevel cell (MLC) storage, modeling, and applications, *Nanoscale Res. Lett.* **15**, 1 (2020).
- [4] C. Ríos, M. Stegmaier, P. Hosseini, D. Wang, T. Scherer, C. D. Wright, H. Bhaskaran, and W. H. P. Pernice, Integrated all-photon non-volatile multi-level memory, *Nat. Photon.* **9**, 725 (2015).
- [5] K. Olejník, V. Schuler, X. Martí, V. Novák, Z. Kašpar, P. Wadley, R. P. Campion, K. W. Edmonds, B. L. Gallagher, J. Garcés, M. Baumgartner, P. Gambardella, and T. Jungwirth, Antiferromagnetic CuMnAs multi-level memory cell with microelectronic compatibility, *Nat. Commun.* **8**, 1 (2017).
- [6] A. N. McCaughan, N. S. Abebe, Q.-Y. Zhao, and K. K. Berggren, Using geometry to sense current, *Nano Lett.* **16**, 7626 (2016).
- [7] Q.-Y. Zhao, E. A. Toomey, B. A. Butters, A. N. McCaughan, A. E. Dane, S.-W. Nam, and K. K. Berggren, A compact superconducting nanowire memory element operated by nanowire cryotrons, *Supercond. Sci. Technol.* **31**, 035009 (2018).
- [8] A. N. McCaughan, E. Toomey, M. Schneider, K. K. Berggren, and S. W. Nam, A kinetic-inductance-based

- superconducting memory element with shunting and sub-nanosecond write times, *Supercond. Sci. Technol.* **32**, 015005 (2018).
- [9] E. Toomey, M. Onen, M. Colangelo, B. A. Butters, A. N. McCaughan, and K. K. Berggren, Bridging the Gap Between Nanowires and Josephson Junctions: A Superconducting Device Based on Controlled Fluxon Transfer, *Phys. Rev. Appl.* **11**, 034006 (2019).
- [10] M. Tinkham, *Introduction to Superconductivity* (McGraw-Hill Book Co., New York, 1996), 2nd ed.
- [11] J. Clarke, Principles and applications of SQUIDs, *Proc. IEEE* **77**, 1208 (1989).
- [12] C. P. Foley and H. Hilgenkamp, Why nanoSQUIDs are important: an introduction to the focus issue, *Supercond. Sci. Technol.* **22**, 064001 (2009).
- [13] C. Granata and A. Vettoliere, Nano superconducting quantum interference device: A powerful tool for nanoscale investigations, *Phys. Rep.* **614**, 1 (2016).
- [14] M. Kjaergaard, M. E. Schwartz, J. Braumüller, P. Krantz, J. I.-J. Wang, S. Gustavsson, and W. D. Oliver, Superconducting qubits: Current state of play, *Annu. Rev. Condens. Matter Phys.* **11**, 369 (2020).
- [15] K. Hasselbach, D. Mailly, and J. R. Kirtley, Microsuperconducting quantum interference device characteristics, *J. Appl. Phys.* **91**, 4432 (2002).
- [16] G. J. Podd, G. D. Hutchinson, D. A. Williams, and D. G. Hasko, Micro-SQUIDs with controllable asymmetry via hot-phonon controlled junctions, *Phys. Rev. B* **75**, 134501 (2007).
- [17] A. Murphy and A. Bezryadin, Asymmetric nanowire SQUID: Linear current-phase relation, stochastic switching, and symmetries, *Phys. Rev. B* **96**, 094507 (2017).
- [18] H. Dausy, L. Nulens, B. Raes, M. J. Van Bael, and J. Van de Vondel, Impact of Kinetic Inductance on the Critical-Current Oscillations of Nanobridge SQUIDs, *Phys. Rev. Appl.* **16**, 024013 (2021).
- [19] C. N. Lau, N. Markovic, M. Bockrath, A. Bezryadin, and M. Tinkham, Quantum Phase Slips in Superconducting Nanowires, *Phys. Rev. Lett.* **87**, 217003 (2001).
- [20] J. E. Mooij and Y. V. Nazarov, Superconducting nanowires as quantum phase-slip junctions, *Nat. Phys.* **2**, 169 (2006).
- [21] T. Aref, A. Levchenko, V. Vakaryuk, and A. Bezryadin, Quantitative analysis of quantum phase slips in superconducting $\text{Mo}_7\text{Ge}_{24}$ nanowires revealed by switching-current statistics, *Phys. Rev. B* **86**, 024507 (2012).
- [22] A. Murphy, P. Weinberg, T. Aref, U. C. Coskun, V. Vakaryuk, A. Levchenko, and A. Bezryadin, Universal Features of Counting Statistics of Thermal and Quantum Phase Slips in Nanosize Superconducting Circuits, *Phys. Rev. Lett.* **110**, 247001 (2013).
- [23] A. Belkin, M. Belkin, V. Vakaryuk, S. Khlebnikov, and A. Bezryadin, Formation of Quantum Phase Slip Pairs in Superconducting Nanowires, *Phys. Rev. X* **5**, 021023 (2015).
- [24] V. Lefevre-Seguin, E. Turlot, C. Urbina, D. Esteve, and M. H. Devoret, Thermal activation of a hysteretic dc superconducting quantum interference device from its different zero-voltage states, *Phys. Rev. B* **46**, 5507 (1992).
- [25] T. A. Palomaki, S. K. Dutta, H. Paik, H. Xu, J. Matthews, R. M. Lewis, R. C. Ramos, K. Mitra, P. R. Johnson, F. W. Strauch, and A. J. Dragt, Initializing the flux state of multiwell inductively isolated Josephson junction qubits, *Phys. Rev. B* **73**, 014520 (2006).
- [26] E. Ilin, X. Song, I. Burkova, A. Silge, Z. Guo, K. Ilin, and A. Bezryadin, Supercurrent-controlled kinetic inductance superconducting memory element, *Appl. Phys. Lett.* **118**, 112603 (2021).
- [27] J. E. Mooij and C. J. P. M. Harmans, Phase-slip flux qubits, *New J. Phys.* **7**, 219 (2005).
- [28] L. Chen, L. Wu, Y. Wang, Y. Pan, D. Zhang, J. Zeng, X. Liu, L. Ma, W. Peng, Y. Wang, J. Ren, and Z. Wang, Miniaturization of the superconducting memory cell via a three-dimensional Nb nano-superconducting quantum interference device, *ACS Nano* **14**, 11002 (2020).
- [29] Y. Takeshita, F. Li, D. Hasegawa, K. Sano, M. Tanaka, T. Yamashita, and A. Fujimaki, High-speed memory driven by SFQ pulses based on $0-\pi$ SQUID, *IEEE Trans. Appl. Supercond.* **31**, 1 (2021).
- [30] N. Ligato, E. Strambini, F. Paolucci, and F. Giazotto, Preliminary demonstration of a persistent Josephson phase-slip memory cell with topological protection, *Nat. Commun.* **12**, 1 (2021).
- [31] L. Nulens, H. Dausy, M. J. Wyszynski, B. Raes, M. J. Van Bael, M. V. Milošević, and J. Van de Vondel, Metastable states and hidden phase slips in nanobridge SQUIDs, *Phys. Rev. B* **106**, 134518 (2022).
- [32] A direct inspection of the measured $I_c(B)$ distribution for device 400a does not reveal the full shape of the vorticity diamond used to describe the critical-current oscillation as only one of the branches appears. For this reason, we employ the preparation protocol explained in Sec. III to obtain data relative to both diamond branches for device 400a.
- [33] A. Murphy, D. V. Averin, and A. Bezryadin, Nanoscale superconducting memory based on the kinetic inductance of asymmetric nanowire loops, *New J. Phys.* **19**, 063015 (2017).
- [34] Here, the measured critical-current values differ from those presented in Fig. 1(b) because the device is removed from the experimental setup for approximately 1 month, which slightly depletes its superconducting properties.